M.S. KARAKAŞ*[#], A. GÜNEN**, E. KANCA***, E. YILMAZ****

BORIDE LAYER GROWTH KINETICS OF AISI H13 STEEL BORIDED WITH NANO-SIZED POWDERS

Growth kinetics of boride layers in AISI H13 steel was investigated using the pack boriding method at temperatures of 1073, 1173 and 1273 K (800°C, 900°C and 1000°C) for periods of 2, 4 and 6 h with nano-sized boron (NB) and micron-sized Ekabor II powders as boriding agents. The total thickness of the boride layer (including both FeB and Fe_2B) after boriding at 1273 K (1000°C) for 6 h was 103.8 μm and 96.5 μm for the NB and Ekabor II specimens, respectively. X-ray diffraction analysis of the boride layers on the surfaces borided with NB and Ekabor II revealed the presence of FeB and Fe_2B phases with sawtooth morphology. The FeB/Fe_2B volume ratio was higher in the specimens borided with NB. The thickness of the boride layer (FeB + Fe_2B) increased with the increasing boriding temperature and time. The FeB layer in the NB specimen displayed a (002) preferred orientation.

Keywords: Boriding, growth kinetics, activation energy

1. Introduction

Boriding (also known as boronizing) is a thermochemical surface hardening process in which boron atoms are diffused into the surface of a workpiece to form single- or multi-phase boride layers with the base metal. The process can be carried out in a solid, liquid or gaseous medium. Among these processing routes, solid-state pack boriding is the most frequently used technique [1,2]. The powder pack usually contains a source for boron (such as boron carbide or amorphous boron), an activator, and a diluent.

Pack boriding of ferrous alloys is generally carried out between temperatures of 1073 K and 1323 K (800°C and 1050°C) which usually results in the formation of either a single-phase layer of Fe_2B or a dual-phase layer consisting of FeB and Fe_2B [3]. The characteristic sawtooth or serrated morphology of the boride layer is dominant in plain carbon and low alloy steels. Between the formation of a single- or dual-phase boride layer, single-phase Fe_2B layer formation is almost always preferred. The main reason for this is the flaking/spalling that may occur in the dual-phase boride layer. The FeB and Fe_2B phases within the bilayer exhibit substantially different coefficients of thermal expansion ($\alpha_{FeB} = 23 \times 10^{-6}$ K^{-1} versus $\alpha_{Fe2B} = 7.65 \times 10^{-6}$ K^{-1}), which may lead to microcracking at the FeB/Fe_2B interface when a force is applied. Therefore, despite the fact that FeB has greater hardness [1], its formation is often considered undesir-

able. Methods for preventing the formation of FeB are based on decreasing the potential of the boriding process, i.e. diluting the boriding agent in the boriding pack, which has the drawback of increased processing time. Recent studies have shown that a heat treatment at high temperatures can lead to the transformation of FeB to Fe_2B [4,5]. Such a heat treatment can reduce or eliminate the disadvantages of FeB formation, but nevertheless adds another processing step to the boriding treatment. The overall thickness of the boride layer formed on the surface (also known as the case depth) depends on temperature, duration, the boron potential of the powder pack, as well as the chemical composition of the alloy. A few studies have shown that the particle size of the boriding powders can also have a significant influence on the growth of the boride layers [6-9].

In the present work, the growth of boride layers in AISI H13 steel was investigated by boriding treatments using two separate powder pack mixtures: one containing micron-sized boron carbide and the other containing nano-sized amorphous boron as the boriding source. Boriding treatments were conducted at different processing temperatures and durations to determine kinetic parameters. Scanning electron microscopy (SEM) was used to examine and compare the resulting microstructures. Hardness tests were made to compare the hardnesses of the phases formed, and X-ray diffraction (XRD) was used to identify the phase composition of the boride layers. An empirical model was developed for estimating the boride layer thickness.

* SELCUK UNIVERSITY, FACULTY OF ENGINEERING, DEPARTMENT OF METALLURGICAL AND MATERIALS ENGINEERING, KONYA 42130, TURKEY
** ISKENDERUN TECHNICAL UNIVERSITY, FACULTY OF ENGINEERING AND NATURAL SCIENCES, DEPARTMENT OF METALLURGICAL AND MATERIALS ENGINEERING, HATAY 31200, TURKEY
*** ISKENDERUN TECHNICAL UNIVERSITY, FACULTY OF ENGINEERING AND NATURAL SCIENCES, DEPARTMENT OF MECHANICAL ENGINEERING, HATAY 31200, TURKEY
**** CANKAYA UNIVERSITY, FACULTY OF ENGINEERING, DEPARTMENT OF MATERIALS SCIENCE AND ENGINEERING, ANKARA 06790, TURKEY
# Corresponding author: skarakas@selcuk.edu.tr

2. Experimental method

The substrate used in this study was an AISI H13 (5.20 wt.% Cr, 1.40 wt.% Mo, 1.0 wt.% V, 0.8 wt.% Si, 0.40 wt.% C, 0.2 wt.% Mn and balance Fe) hot work tool steel. Two different boriding agents were used. The first consisted of 90 vol.% amorphous boron powders (NaBond Technologies Co. Ltd., Kowloon, Hong Kong) prepared by mechanical milling with particle size ranging between 50 and 100 nm as the boriding source and 10 vol.% $NaBF_4$ (Sigma-Aldrich, Schnelldorf, Germany) as the activator, which will be labeled as nano-boron (NB). The second boriding agent was commercial Ekabor II (BorTech GmbH, Hürth, Germany), which consists of 5% B_4C as the boriding source, 5% KBF_4 as the activator, and 90% SiC as the diluent. Particle sizes were determined using a Malvern Mastersizer 2000 (Malvern, Worcestershire, UK), equipped with Hydro2000S dispersion units. Each sample was ground up to 1200 grit SiC paper then washed in distilled water and ultrasonically cleaned in acetone before the boriding treatment. The samples were then packed with the boriding powder in a stainless steel container and the top of the container was covered with very fine SiC powders to prevent oxidation. The boriding process was carried out at temperatures of 1073 K, 1173 K and 1273K (800°C, 900°C and 1000°C) for 2, 4 and 6 h, and then borided samples were removed from the furnace and cooled to room temperature in air. A fresh boriding agent used for boriding each sample.

The borided samples were cut to dimensions of 20 × 20 × 5 mm. The cross-sections of the specimens were cold mounted and ground with up to 1500 grit SiC papers and polished with 3 μm alumina paste followed by 1 μm diamond paste to achieve a good mirror finish. After polishing, the samples were etched in a 3% Nital solution to reveal fine microstructural details.

Metallographic studies were conducted on the polished and etched cross-sections of the specimens using a Zeiss Ultra Plus field emission scanning electron microscope (FESEM) equipped with Energy Dispersive Spectroscopy (EDS) capability, operating at an accelerating voltage of 25 kV. Due to the complex shape of the boride layer, thickness measurements were made using the method described by Yu et al. [9], which takes into account the thickness of the boride needles. The average thickness of the boride layer, d, was calculated using the equation

$$d = \frac{A}{w} \tag{1}$$

where A and w indicate the area and width of the boride layer, respectively. Image-processing software was utilized to calculate the area and length of the boride layer. A schematic illustrating the measurement procedure is given in Fig. 1. A sample microstructure of the boride coating is also shown in the figure, demonstrating the jagged and discontinuous nature of the boride/substrate interface.

Microhardness measurements were recorded using a Future-Tech FM-700 hardness tester using 100 g load and 10 s dwell time. The thicknesses of boride layers were determined by FESEM and the presence of the boride phases formed on the
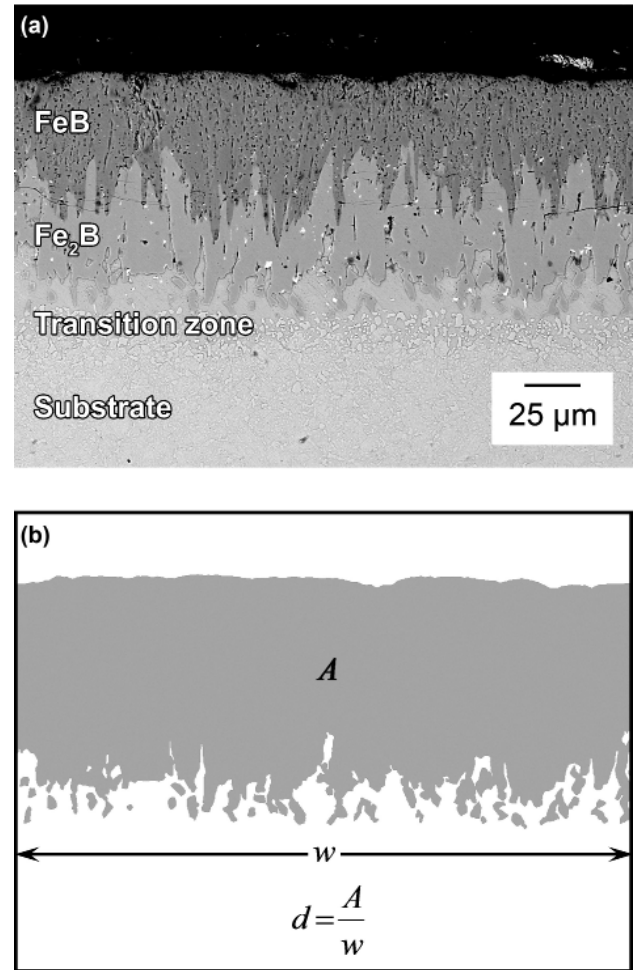

Fig. 1. Schematic showing the measurement procedure for estimating the boride layer thickness (the microstructure shown is that of the specimen borided with Ekabor II powders at 1273 K (1000°C) for 6 h)

surface was confirmed by X-ray diffraction (XRD) analyses using a computer-controlled Rigaku Ultima IV with Cu Kα radiation (λ_{Cu} = 0.1540 nm) with 2θ angles ranging from 10° to 90°.

3. Results and discussion

3.1. Microstructures of the borided specimens

Boron has higher chemical potential compared to boron carbide; it is to be expected therefore that FeB will more likely form in samples borided with NB powders compared to Ekabor II powders. SEM micrographs from cross-sections of specimens borided with NB and Ekabor II powders at different processing times and temperatures are presented in Figs. 2,3, respectively. The layers formed on the borided specimens have a sawtooth morphology, which is commonly observed in borided steels. Three distinct regions are identified on cross-sections of the borided specimens, regardless of the boriding agent: (a) the boride layer, consisting of FeB and Fe_2B phases; (b) the transition zone in which carbon is diffused away from the boride layer and into the substrate; and (c) the substrate essentially unaffected by

boron diffusion (Fig. 1). The boride layers formed on the H13 steel display less sawtooth morphology compared to borides formed on plain carbons steels due to alloying elements. Higher FeB/Fe$_2$B thickness ratios are evident in the NB specimens (thickness ratios are 2.11 and 1.23 for the NB and Ekabor II specimens, respectively, for specimens borided at 1273 K (1000°C) for 6 h). The increase in contacting surface area and decrease in diffusion distance provided by the nanoparticles accelerated the diffusion of boron into the substrate material, resulting in higher FeB/Fe$_2$B thickness ratios in the NB specimens.
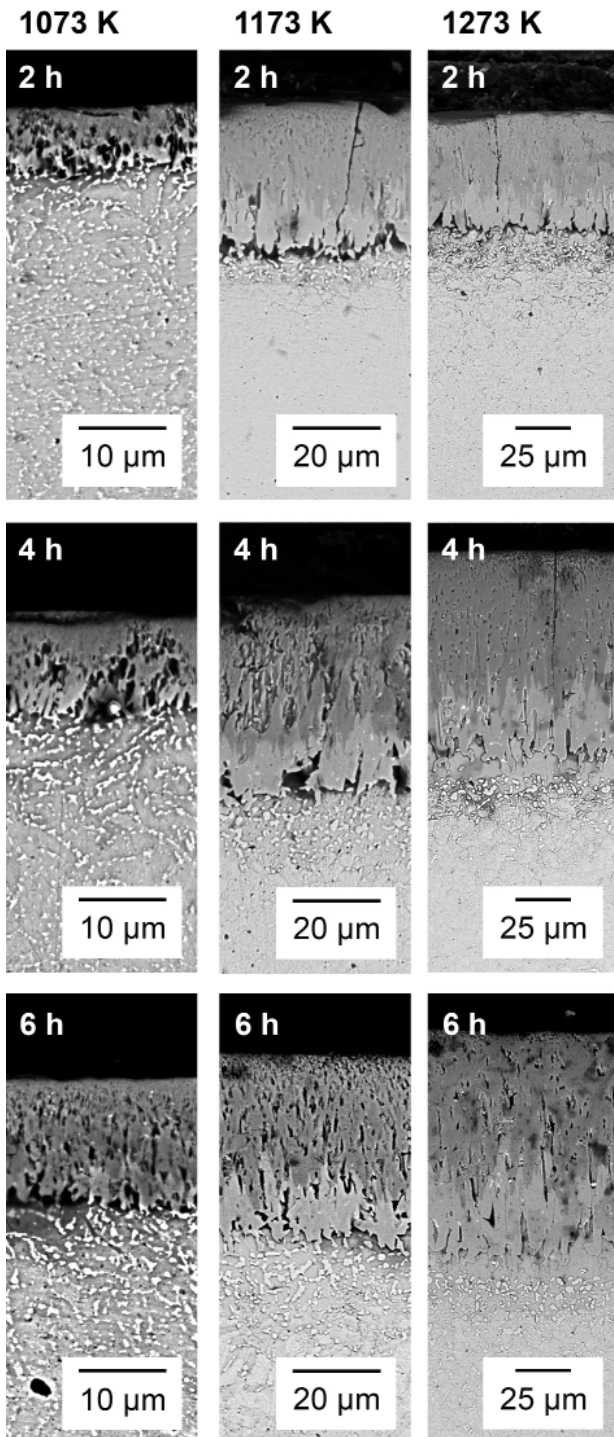

Fig. 2. Microstructures of specimens borided with NB powders at different processing times and temperatures
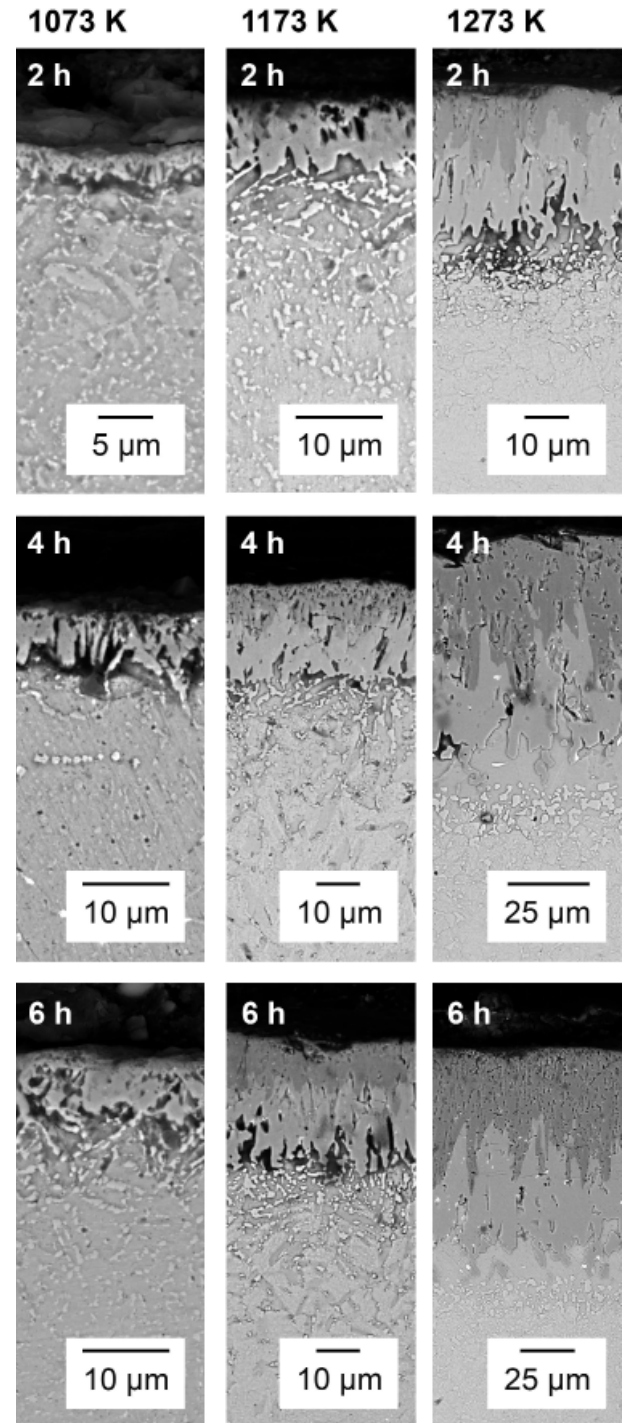

Fig. 3. Microstructures of specimens borided with Ekabor II powders at different processing times and temperatures

Figure 4 shows a graphical representation of the variation of the square of boride layer thickness with boriding temperature and time obtained from optical and SEM photographs. Increasing temperature and increasing time both have the effect of increasing the thickness of the boride layer, due to increasing boron diffusion. The maximum boride layer thickness values are obtained at 1273 K (1000°C) for 6 h, which are 103.8 μm and 96.5 μm for the NB and Ekabor II specimens, respectively. The curves for Ekabor II display a more linear growth compared to the curves for NB.
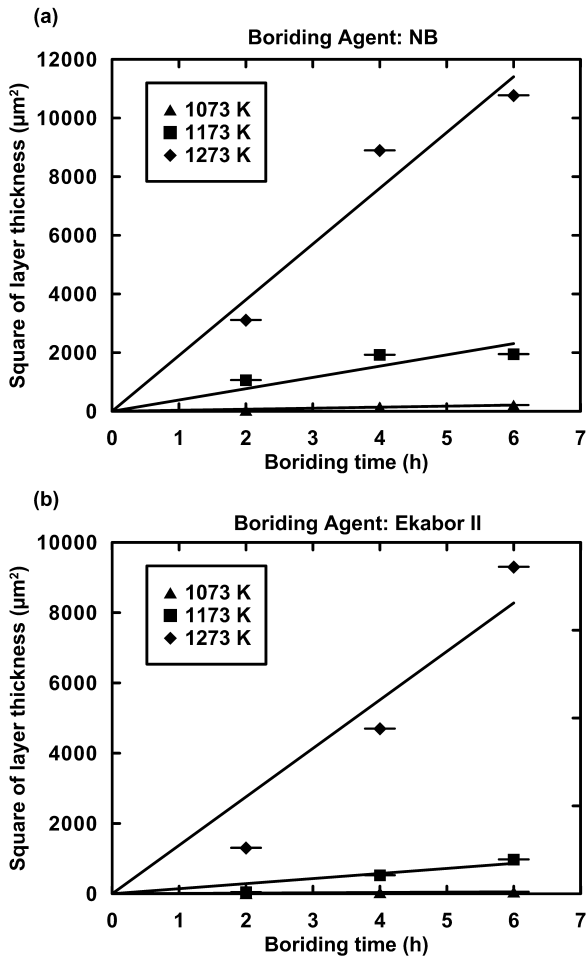
Fig. 4. The square of the average boride layer thickness showing the range of growth of the boride layer for the specimens as a function of process time using (a) NB powders and (b) Ekabor II powders as boriding agents

Fig. 5. Hardness profiles for specimens borided with NB powders at (a) 1173 K (900°C) and (b) 1273 K (1000°C)

3.2. Hardness tests

Hardness profiles for the specimens borided with NB and Ekabor II powders are shown in Figs. 5,6, respectively. The average hardness of the FeB layer which forms on the outer surface is about 2000 HV for both specimens, approximately 3.75 times harder than the substrate which has a hardness of about 530 HV. The hardness of the Fe_2B layer lies between 1600 and 1800 HV. Although hardness measurements of thin films on soft substrates are always subject to inaccuracies [10], the measurements conducted indicate the higher hardness of FeB compared to Fe_2B.

3.3. XRD measurements

The representative XRD patterns of the top surface layers of the specimens borided at 1173 K for 6 h with NB and Ekabor II powders are presented in Fig. 7. Both specimens display diffraction peaks for FeB, however diffraction peaks for Fe_2B are only visible in the Ekabor II specimen. This does not necessarily mean that Fe_2B was absent in the NB samples, since Fig. 2 clearly shows a double-layered boride coating in the 1173 K (900°C) and
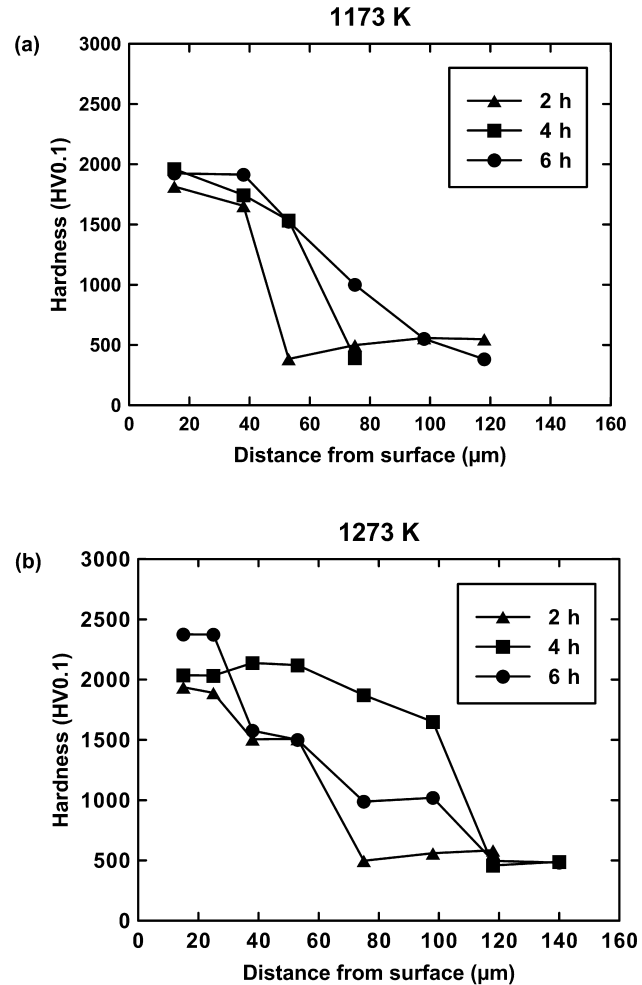
1273 K (1000°C) specimens. The X-rays were unable to penetrate much beyond the FeB layer, and this shallow penetration depth led to the reading of only FeB on the specimen surface. Moreover, the NB specimen only shows one strong peak which belongs to the (002) diffraction peak for FeB, indicating that the FeB phase exhibits a strong (002) preferred orientation. The preferred (002) growth texture for both FeB and Fe_2B has been reported previously in the literature [11-13]. The low noise-to-signal ratio in the NB specimen indicates good crystallinity, whereas the high noise-to-signal ratio in the Ekabor II specimen suggests more inelastic scattering/absorbance and less crystallinity.

3.4. Boride kinetics

Parameters such as processing temperature and time have to be known in order to control the boriding process. The main factor driving the growth of boride layer is the diffusion of boron into the substrate. The growth of the boride layer obeys a parabolic growth law, and the square of the boride layer thickness synthesized by the boriding treatment can be described as follows:
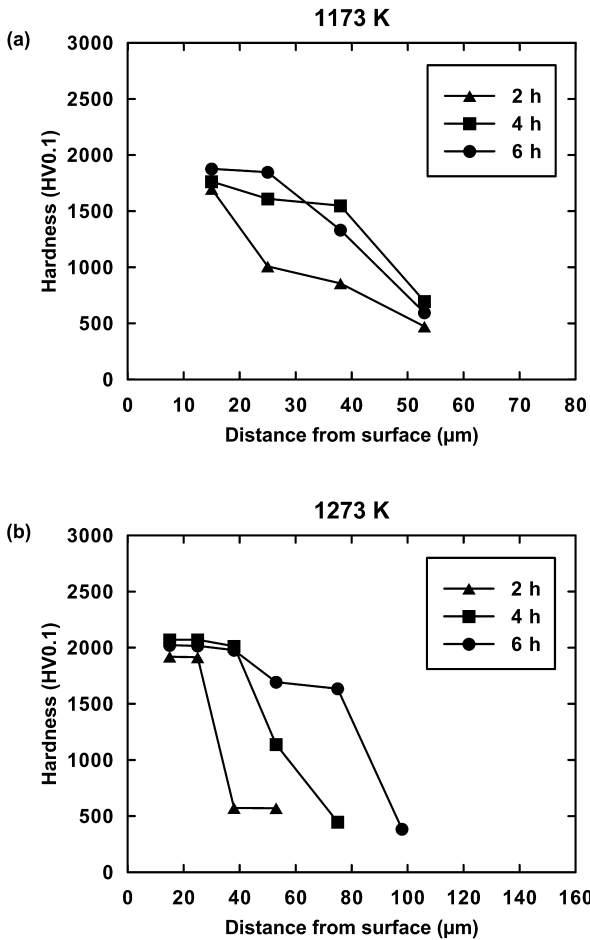
$$d^2 = Kt \tag{2}$$

Fig. 6. Hardness profiles for specimens borided with Ekabor II powders at (a) 1173 K (900°C) and (b) 1273 K (1000°C)
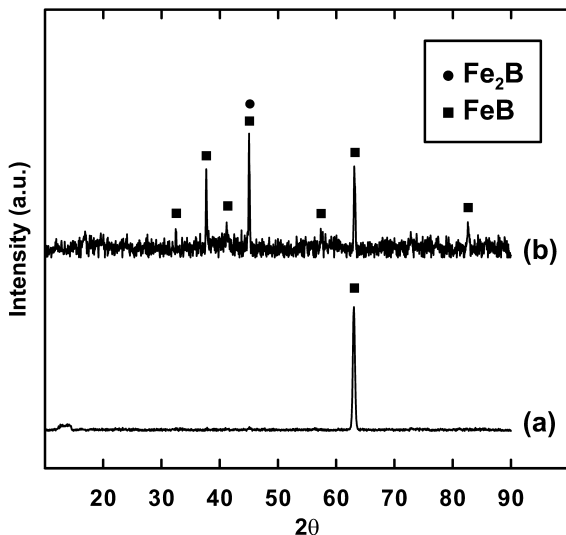

Fig. 7. Diffraction patterns for the specimens borided at 1173 K (900°C) for 6 h with (a) NB and (b) Ekabor II powders

where d is the thickness of boride layer (m), t is the boriding time (s), and K is the growth rate constant with respect to boriding temperature (m²/s). From the thickness-time data shown in Fig. 3, the growth rate constant of the boride layer was calculated.

The growth rate constant K is temperature dependent, and can be described by an Arrhenius equation of the form:

$$K = K_0 \exp\left(\frac{-Q}{RT}\right) \qquad (3)$$

where K_0 is the collision factor (m²/s) and is an indicator of the effective collisions between reactive species, Q is the activation energy for the particular reaction (J/mol), T is the absolute temperature (K) and R is the universal gas constant (J/(mol·K)). By taking the natural logarithm of both sides of this equation, we obtain a linear relationship. When $\ln K$ is plotted with respect to the reciprocal of absolute temperature, the activation energy Q and collision factor K_0 can be calculated from the slope and y-intercept, respectively. The $\ln K$ versus $1/T$ plots are shown in Fig. 8, and the values calculated for Q and K_0 are listed in Table 1. The calculated activation energy for the NB specimen (227.5 kJ/mol) is lower than that for the Ekabor II specimen (284.2 kJ/mol), and the activation energy values for both specimens are relatively higher than the values published in the literature [14-26]. A comparison of the activation energies found in the present study and other studies in the literature are given in Table 2. There are several reasons that may have caused this discrepancy, which include the method used for measuring the thickness of the boride layer, the methods used for surface
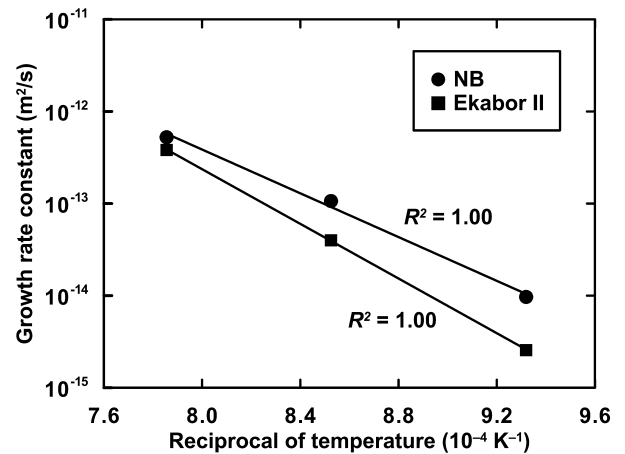

Fig. 8. Growth rate constants of specimens borided with NB and Ekabor II powders as a function of reciprocal of temperature

TABLE 1

Calculated growth rate constants, activation energies and collision factors for the H13 steels borided with NB and Ekabor II powders as a function of boriding temperature

Boriding powder	Temperature, T (K)	Growth rate constant, K (m²/s)	Activation energy, Q (kJ/mol)	Collision factor, K_0 (m²/s)
NB	1073 K	9.73×10^{-15}	227.5	1.25×10^{-3}
	1173 K	1.07×10^{-13}		
	1273 K	5.28×10^{-13}		
Ekabor II	1073 K	2.57×10^{-15}	284.2	1.77×10^{-1}
	1173 K	4.00×10^{-14}		
	1273 K	3.83×10^{-13}		

Comparison of the activation energies

Material	Boriding method	Temperature range, T (K)	Activation energy, Q (kJ/mol)	Phase Composition	Reference
AISI H13	Pack	1123-1273	233	Fe_2B	Keddam et al. (2015) [14]
AISI H13	Pack	1123-1223	185.7	$FeB+Fe_2B$	Boonplook et al. (2014) [15]
AISI H13	Pack	1023-1123	209.4	$Fe_2B(+Fe_2O_3)$	Yang et al. (2014) [16]
AISI H13	Pack	1073-1273	186.2	$FeB+Fe_2B$	Genel (2006) [17]
AISI M2	Pack	1123-1223	240.3	$FeB+Fe_2B$	Ozbek et al. (2011) [18]
AISI P20	Pack	1073-1223	200.0	$FeB+Fe_2B$	Uslu et al. (2007) [19]
AISI 1040	Pack	1073-1223	168.0	$FeB+Fe_2B$	Uslu et al. (2007) [19]
AISI D2	Pack	1123-1273	201.5	Fe_2B	Ortiz-Domínguez et al. (2014) [20]
AISI 316	Pack	1073-1223	199.5	Fe_2B	Ozdemir et al. (2009) [21]
AISI 5140	Slurry salt bath	1073-1273	223	$FeB+Fe_2B$	Sen et al. (2005) [22]
AISI 4340	Slurry salt bath	1073-1273	234	$FeB+Fe_2B$	Sen et al. (2005) [22]
AISI 1045	Slurry salt bath	1073-1273	170	$FeB+Fe_2B$	Sen et al. (2005) [22]
AISI 1045	Paste	1193-1273	226.7	Fe_2B	Campos et al. (2005) [23]
AISI 1018	Electrochemical	1123-1273	172.8	$FeB+Fe_2B$	Kartal et al. (2011) [24]
AISI D2	Electrochemical	1123-1273	137.9	$FeB+Fe_2B$	Sista et al. (2011) [25]
Mild steel	Spark plasma sintering	973-1273	145.8	$FeB+Fe_2B$	Yu et al. (2002) [26]
AISI H13	Pack	1073-1273	227.5, 284.2	$FeB+Fe_2B$	Present study

preparation, the type and size of the boriding powders, the pack thickness, the type of material used for containing the powder pack, possible spalling of the FeB layer, and the temperature ranges studied [27,28]. It should be noted that the boron potential in the boriding medium can have a significant effect on the phase composition of the boride layer, for example FeB formation was not observed in some of the studies listed in Table 2 due to insufficient boron potential for FeB formation [14,20,21,23].

From the calculated values of Q and K_0, empirical equations for the thickness of the boride layer can be derived for the boriding of the AISI H13 steel with either of the boriding agents, given the time and temperature.

For the NB specimen:

$$d = 3.5 \times 10^{-2} \sqrt{t \exp\left(-\frac{27368}{T}\right)} \quad 1073\,\mathrm{K} \leq T \leq 1273\,\mathrm{K} \quad (4)$$

For the Ekabor II specimen:

$$d = 0.42 \sqrt{t \exp\left(-\frac{34179}{T}\right)} \quad 1073\,\mathrm{K} \leq T \leq 1273\,\mathrm{K} \quad (5)$$

Where d is the thickness of the borided layer (m), t is the boriding time (s) and T is the boriding temperature (K).

4. Conclusions

Boride coatings were grown on the surface of AISI H13 steel specimens using two boriding powder mixtures of different composition. The boriding treatment was carried out at temperatures of 1073, 1173 and 1273 K with different treatment durations to compare the growth rates and mechanisms. Growth of FeB and Fe_2B phases was observed with both powder mixtures, and in both cases the boride bilayer displayed a sawtooth morphology. The competition between FeB and Fe_2B was controlled by the boron potential in the boriding media. Use of powder mixtures with nanoparticles of higher boron potential resulted in a reduction in the activation energy of the boriding treatment (227.5 kJ/mol for NB compared to 284.2 kJ/mol for Ekabor II), and also led to higher FeB/Fe_2B layer thickness ratios. A very strong (002) orientation was detected in the FeB layer when the boron potential of the boriding medium was high.

REFERENCES

[1] A.K. Sinha, Boriding (boronizing) of metals in: ASM Handbook Volume 4 Heat Treating 1991 ASM, Metals Park, OH.

[2] J.R. Davis, Surface Hardening Of Steels: Understanding the Basics, 2002 ASM, Metals Park, OH.

[3] F.C. Campbell, Elements of Metallurgy and Engineering Alloys, 2008 ASM, Metals Park, OH.

[4] V.I. Dybkov, J. Mater. Sci. **42**, 6614-6627 (2007).

[5] W. Fichtl, Mater. Des. **2**, 276-286 (1981).

[6] H.A.M. Yusof, I. Jauhari, S. Rozali, O. Hiroyuki, Key Eng. Mater. **345-346**, 601-604 (2007).

[7] C. Meriç, S. Sahin, S.S. Yilmaz, Mater. Res. Bull. **35**, 2165-2172 (2000).

[8] A. Calik, ISIJ Int. **53**, 160-164 (2013).

[9] L.G. Yu, X.J. Chen, K.A. Khor, G. Sundararajan, Acta Mater. **53**, 2361-2368 (2005).

[10] B. Jonsson, S. Hogmark, Thin Solid Films **114**, 257-269 (1984).

[11] H. Kunst, O. Schaaber, Härt.-Tech. Mitt. **22**, 275-292 (1967).

[12] G. Palombarini, M. Carbucicchio, J. Mater. Sci. Lett. **6**, 415-416 (1987).

[13] E. Campos-Silva, G.A. Rodríguez-Castro, Boriding To Improve The Mechanical Properties And Corrosion Resistance Of Steels in: J. Mittemeijer and Marcel A. J. Somers (Eds.), Thermochemical Surface Engineering Of Steels, 2015 Woodhead, Cambridge, UK.

[14] M. Keddam, M. Ortiz-Dominguez, M. Elias-Espinosa, O. Damian-Mejia, A. Arenas-Flores, O.A. Gomez-Vargas , M. Abreu-Quijano, J.I. Aldana-Gonzalez, J. Zuno-Silva, Trans. Indian Inst. Met. **68**, 433-442 (2015).

[15] Y. Boonplook, P. Juijerm, Adv. Mater. Res. **931-932**, 296-300 (2014).

[16] H. Yang, X. Wu, Z. Yang, S. Pu, H. Wang, J. Alloys Compd. **590**, 388-395 (2014).

[17] K. Genel, Vacuum **80**, 451-457 (2006).

[18] I. Ozbek, C. Bindal, Vacuum **86**, 391-397 (2011).

[19] I. Uslu, H. Comert, M. Ipek, F.G. Celebi, O. Ozdemir, C. Bindal, Mater. Des. **28**, 1819-1826 (2007).

[20] M. Ortiz-Domínguez, M. Keddam, M. Elias-Espinosa, O. Damián-Mejía, M.A. Flores-Rentería, A. Arenas-Flores, J. Hernández-Ávila, Surf. Eng. **30**, 490-497 (2014).

[21] O. Ozdemir, M.A. Omar, M. Usta, S. Zeytin, C. Bindal, A.H. Ucisik, Vacuum **83**, 175-179 (2008).

[22] S. Sen, U. Sen, C. Bindal, Surf. Coat. Technol. **191**, 274-85 (2005).

[23] I. Campos, O. Bautista, G. Ramirez, M. Islas, J. De La Parra, L. Zuniga, Appl. Surf. Sci. **243**, 429-436 (2005).

[24] G. Kartal, O.L. Eryilmaz, G. Krumdick, A. Erdemir, S. Timur, Appl. Surf. Sci. **257**, 6928-6934 (2011).

[25] V. Sista, O. Kahvecioglu, O.L. Eryilmaz, A. Erdemir, S. Timur, Thin Solid Films **520**, 1582-1588 (2011).

[26] L.G. Yu, K.A. Khor, G. Sundararajan, Surf. Coat. Technol. **157**, 226-230 (2002).

[27] V. Jain, G. Sundararajan, Surf. Coat. Technol. **149**, 21-26 (2002).

[28] C. M. Brakman, A.W.J. Gommers, E.J. Mittemeijer, J. Mater. Res. **4**, 1354-1370 (1989).